NACE® INTERNATIONAL

Precipitation Kinetics of FeCO₃ in Non-Ideal Solutions

Zheng Ma, Bruce Brown, Srdjan Nesic, and Marc Singer
Institute for Corrosion and Multiphase Technology, Ohio University
342 West State Street
Athens, OH, 45701
USA

ABSTRACT

Precipitation kinetics of FeCO₃ has been previously studied over a range of temperatures from 50ºC to 80ºC, leading to the development of an equation predicting FeCO₃ precipitation rate. However, this initial equation, which depends mostly on calibrated kinetic constant $k_{r,FeCO_3}$, and activation energy, ΔG_{FeCO_3}, was only validated in 1wt.% NaCl aqueous solution. Further testing had shown an over-estimation of FeCO₃ precipitation rate occurred when applying the model to solutions containing higher NaCl content, and thus deviating strongly from ideality. In this research, updated expression of both the kinetic constant $k_{r,FeCO_3}$, and the activation energy, ΔG_{FeCO_3}, were extracted from additional experiments using 3 wt%, 6 wt%, and 9 wt% NaCl solutions at temperatures of 60°C, 70°C, and 80°C. Observations show that strong deviation from solutions ideality affected both parameters. This led to the development a new version of the kinetic model for FeCO₃ precipitation valid for a wider range of experimental conditions.

Keywords: EQCM, iron carbonate, precipitation kinetics, non-ideal solutions

INTRODUCTION

Corrosion of carbon steel pipelines in oil and gas applications is often divided into two main categories: sweet corrosion that is mainly caused by aqueous carbon dioxide (CO_2), and sour corrosion which is due to aqueous hydrogen sulfide (H_2S).[1] The formation of corrosion product layers plays a key role in governing the corrosion processes. The formed corrosion product layer could be protective and reduce the corrosion rate by serving as a diffusion barrier, or by blocking the corrosion reaction at the metal surface.[2] It has been suggested that the protectiveness of a corrosion product layer is dependent on the competition between the precipitation rate and corrosion rate of the underlying substrate metal.[2-4] Therefore, understanding the factors governing the corrosion product layer formation is an important step in understanding the level of protectiveness it offers. Many efforts have been put into the investigation of iron carbonate ($FeCO_3$) precipitation kinetics,[5-8] as it is the most common corrosion product that can be observed in sweet corrosions. Most of the results were obtained from very diluted solution which do not deviate greatly from ideal solution behavior. However, these experimental data may not describe accurately the precipitation rate of corrosion product formed in field environments

where the aqueous solution is often a complex brine, with properties far removed from an ideal solution. This makes the non-ideality of solutions (i.e., the ionic strength of solutions) an important parameter that needs to be extensively evaluated with respect to corrosion and corrosion product.

For $FeCO_3$ to be precipitated as a corrosion product, its saturation level, S_{FeCO_3}, must be higher than unit.[5, 8.] S_{FeCO_3} is the ratio between species concentration (mol/L) product of $[Fe^{2+}]$ and $[CO_3^{2-}]$, and the solubility product of FeCO₃, $K_{sp,FeCO_3}$, in mol²/L:[2.]

$$S_{FeCO_3} = \frac{c_{Fe^{2+}} c_{CO_3^{2-}}}{K_{sp,FeCO_3}} \tag{1}$$

Where $K_{sp,FeCO_3}$ is dependent on both temperature in Kelvin and ionic strength in solution, I in mol/L, according to Sun and Nesic:[2.]

$$\log K_{sp,FeCO_3} = -59.3498 - 0.041377\, T_K - \frac{2.1963}{T_K} + 24.5724 \log T_K + 2.518\, I^{0.5} - 0.657\, I \tag{2}$$

And where the ionic strength, often used to characterize the non-ideality of solutions, is a function of species concentration c_i in mol/L and the species charge z_i:

$$I = \frac{1}{2} \sum c_i z_i^2 \tag{3}$$

This makes both $K_{sp,FeCO_3}$ and S_{FeCO_3} dependent on ionic strength as well. Equation (2) and Equation (1) respectively show that $K_{sp,FeCO_3}$ increases with the increase of I, and S_{FeCO_3} decreases with the increase of I. Calculation considering 100 ppm $[Fe^{2+}]$, pH 6.6, 0.53 bar CO₂ at 80°C, as an example, are shown in Figure 1 for $K_{sp,FeCO_3}$ and Figure 2 for S_{FeCO_3}. In both calculations, the ionic strength of the solution was adjusted by changing NaCl concentration, which is represented as wt% NaCl. It can be seen that under the above-mentioned given conditions, the $K_{sp,FeCO_3}$ increased in value about 20 times from 1 wt% NaCl solution to 9 wt% NaCl solution, and the S_{FeCO_3} decreased about four times.
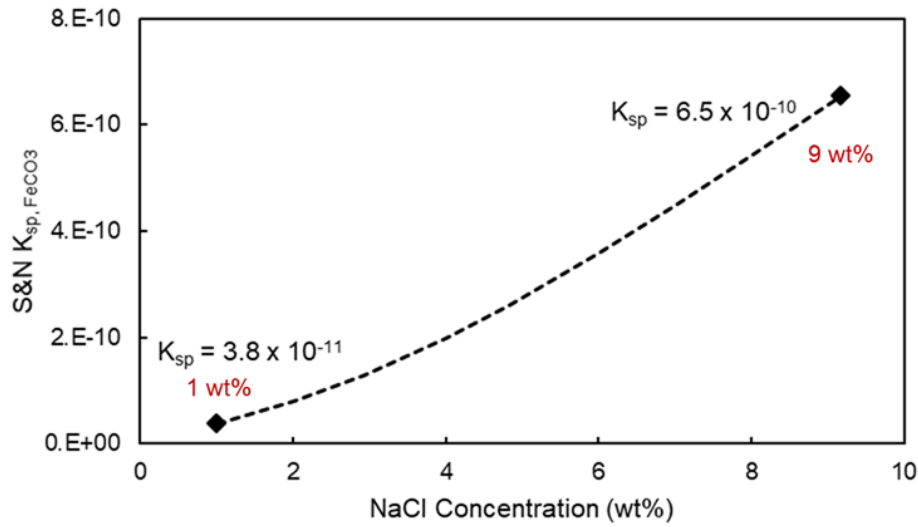
Figure 1. Predicted non-ideality effect on $K_{sp,FeCO_3}$ by Sun and Nesic at 80°C, 100ppm [Fe^{2+}], pH=6.60, and 0.53 bar CO$_2$.
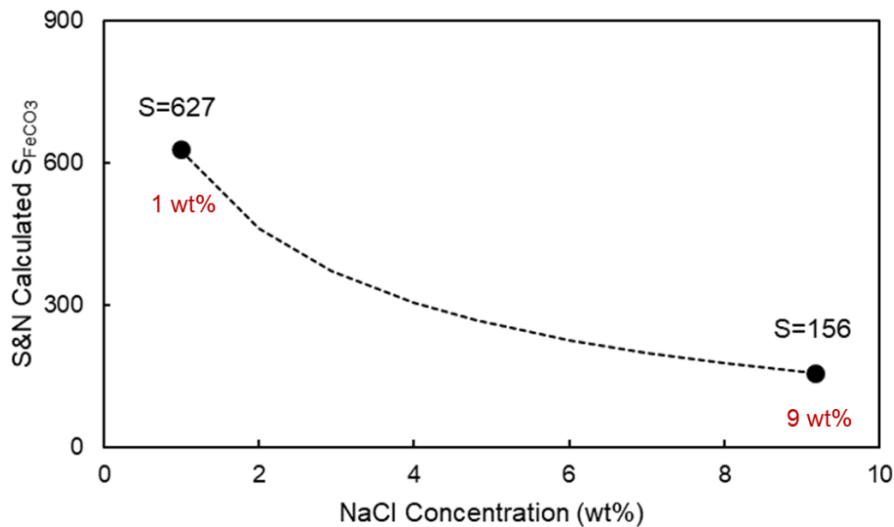

Figure 2. Predicted non-ideality effect on S_{FeCO_3} by Sun and Nesic at 80°C, 100ppm [Fe^{2+}], pH=6.60, and 0.53 bar CO$_2$.

Both S_{FeCO_3} and $K_{sp,FeCO_3}$ affect the precipitation rate of FeCO$_3$ (PR_{FeCO_3}), which is linearly dependent on the product of ($S_{FeCO_3} - 1$) and $K_{sp,FeCO_3}$, based on the theory proposed by Sun and Nesic (S&N Model):[8.]

$$PR_{FeCO_3} = k_{r,FeCO_3} e^{-\left(\frac{\Delta G_{FeCO_3}}{RT}\right)} K_{sp,FeCO_3} (S_{FeCO_3} - 1) \tag{4}$$

This suggests that the ionic strength should also impacts PR_{FeCO_3}. The kinetic constant $k_{r,FeCO_3}$ and the activation energy of FeCO$_3$ precipitation ΔG_{FeCO_3} are constants in this equation, as proposed by Sun and Nesic.[8.] Using the predictions from Figure 1 and Figure 2, PR_{FeCO_3} should increase with the increase of salt concentration, since the increase of $K_{sp,FeCO_3}$ (increases 20 times from 1 wt% NaCl to 9 wt% NaCl) is greater than the decrease of S_{FeCO_3} (decreases four times from 1 wt% NaCl to 9 wt% NaCl). The validity of the prediction for PR_{FeCO_3} also relies on accurate values of $k_{r,FeCO_3}$ and ΔG_{FeCO_3}. However, the values of these two parameters ($\Delta G = 73{,}739$ $J\cdot mol^{-1}$ and $k_r = 3.32 \times 10^7$ $m^4\cdot mol^{-1}\cdot s^{-1}$) were only calibrated in 1 wt% NaCl solution by Ma et.al.[9.] Figure 3 shows the measured PR_{FeCO_3} in aqueous solutions with progressively higher NaCl concentration and the comparison with model predictions. It can be seen clearly that by using values for $k_{r,FeCO_3}$ and ΔG_{FeCO_3} calibrated in 1wt% NaCl solution, Equation (4) does not provide accurate predictions of PR_{FeCO_3} in more concentrated solutions. This suggests that the expression of these two kinetic related parameters needs to be re-evaluated considering different solution ionic strengths to extend the validity of use.
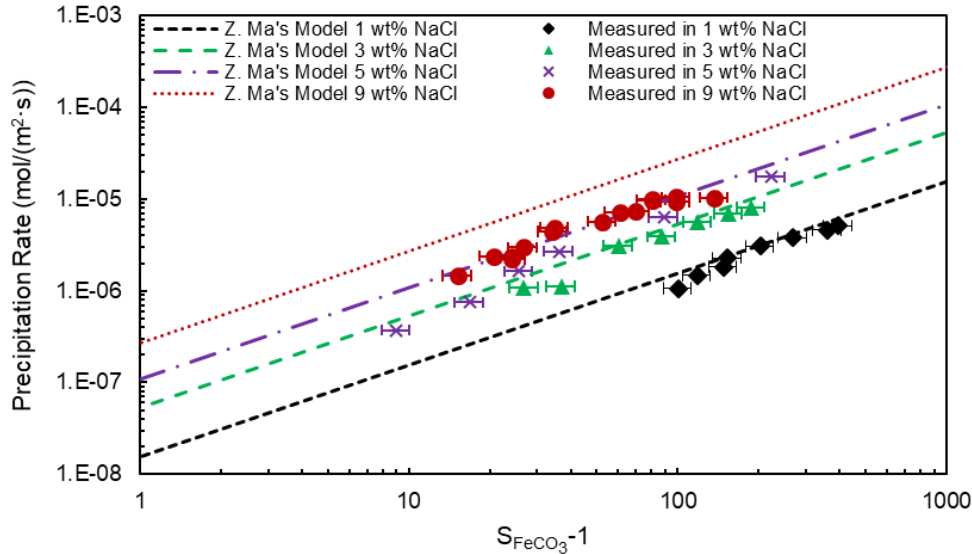

Figure 3. Comparison between model's predictions and measured results in solutions with different NaCl concentrations at 80°C, initial pH=6.60, and 0.53 bar CO₂.

In the current work, a very sensitive device, Electrochemical Quartz Crystal Microbalance (EQCM), was used to monitor the in-situ mass change. The EQCM is a high-resolution mass sensing technique, based upon the piezoelectric effect. Small mass changes, due to the deposition of solid precipitate, are measured on the surface of an oscillating quartz crystal by sensing its oscillation frequency shifts. Theoretically, a nano-scale mass change on the quartz crystal surface leads to a detectable change in its oscillation resonant frequency. According to Sauerbrey's equation,[10.] there is a linear relationship between the mass change on the quartz crystal surface and its resonant frequency change when the formed layer on the crystal surface is thin and rigid neglecting energy dissipation during oscillation):

$$\Delta f = -C_f \cdot \Delta m \tag{5}$$

where the Δf is frequency change (Hz), C_f is the sensitivity factor for the quartz crystal (Hz$\cdot \mu g^{-1}\cdot$ cm^{-2}), and Δm is the change in mass per unit area ($\mu g^{-1}\cdot$ cm^{-2}).

Besides the ability of monitoring the in-situ mass change in high resolution, the EQCM also allows simultaneous electrochemical measurements. This makes the EQCM a good tool for the current work.

<h3 align="center">EXPERIMENTAL</h3>

Methodology

This section presents the methodology developed for using the EQCM for the study of ionic strength effect on the precipitation kinetics of $FeCO_3$. Solutions with different salt (NaCl) concentrations were used to investigate the ionic strength effect on the precipitation kinetics of corrosion products. During precipitation, a cathodic potential was applied on the surface of an iron (Fe) - coated quartz crystal surface. Cathodic polarization was done to ensure that substrate corrosion was minimized and the precipitation of $FeCO_3$ was the dominant process affecting the EQCM measurement. It is understood that the surface pH may increase due to the cathodic polarization and thus lead to a higher precipitation rate. However, it has been proven that the difference of the PR_{FeCO_3} measured from both a polarized surface and an actively corroding surface was negligible due to the relatively high saturation of $FeCO_3$ used in the bulk solution.[9.] In addition, the PR_{FeCO_3} obtained using a polarized surface exhibited good agreement with S&N model's prediction[8].

Apparatus

The EQCM device by Stanford Research System[†] (QCM200) was used. The Fe-coated quartz crystals with a 1.37 cm^2 effective area is shown in Figure 4. Before the experiment, the quartz crystal was installed into the crystal holder and immersed into a 2-liter glass cell (Figure 5, right hand part is a zoomed-in version of the left figure) to serve as the working electrode. A surface to volume (S/V) ratio of 1460 mL/cm^2 was reached, which is sufficiently high to ensure that the precipitation/dissolution of the $FeCO_3$ will not affect the properties of solution.[11.] A saturated Ag/AgCl electrode was used as the reference electrode and the counter electrode was a platinum wire mesh as shown in the figure. The solution pH was monitored through a pH probe immersed in the electrolyte. A desired CO_2 condition was maintained by a sparge tube through the entire duration of the experiment. The temperature of the solution was controlled by an immersed thermocouple connected to a ceramic heating plate.

[†] Trade Name

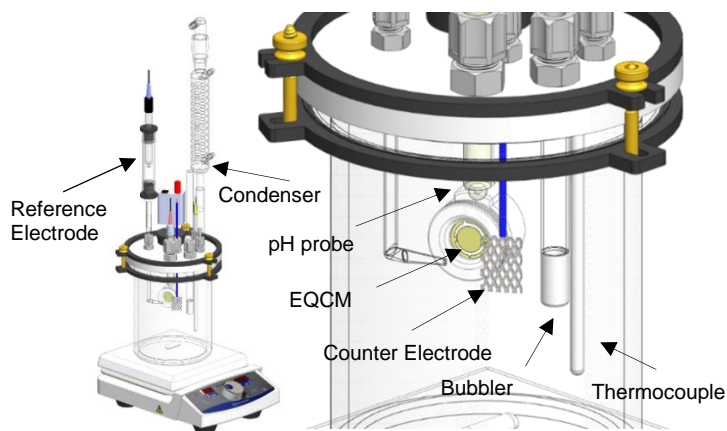**Figure 4: Iron-coated quartz crystal**

Figure 5: Experimental set-up with EQCM (Image courtesy of Cody Shafer, ICMT).

Procedure

The experimental conditions for $FeCO_3$ precipitation in non-ideal solutions are shown in Table 1. All the experiments were conducted in a 2-liter glass cell filled with an aqueous solution containing a specific concentration of NaCl. The solution was de-aerated by sparging with CO_2 for at least two hours ahead of any test and was maintained through the entire duration of the experiment to ensure the oxygen concentration in the solution was lower than 20 ppb. After the solution temperature was set to the desired value, the solution pH was adjusted to 6.60 by adding a deoxygenated $NaHCO_3$ solution. The value of the solution pH is typical of environments encountered in oil and gas production (5 to 7) but was also selected to ensure that relatively high $FeCO_3$ saturation values could be achieved easily. The quartz crystal was cleaned with a N_2 gas stream before each test to remove any dust from the surface. The working electrode potential was adjusted using a potentiostat (Gamry Reference 600™†). A deaerated ferrous chloride ($FeCl_2 \cdot 4H_2O$) solution was added to adjust the Fe^{2+} concentration and S_{FeCO_3}. High initial [Fe^{2+}] was used in the current study to ensure that the solution was highly supersaturated,

---

† Trade Name

and the entire process was accelerated by the high operating temperature (60°C - 80°C). During the measurement, the bulk solution pH was measured *in situ* and solution samples were drawn periodically from the glass cell to record the change Fe^{2+} concentration.

Table 1
Experimental Matrix for FeS Precipitation on Different Substrates.

Description	Parameters
Total pressure / bar	1
Sparge gas	CO_2
Temperature /°C	60 – 80
Initial solution pH	6.60 ± 0.05
Materials	Polished Fe-coated quartz crystal
Stir bar speed / rpm	50
Initial [Fe^{2+}] / ppm	100~150
NaCl Solution	1 wt%, 3 wt%, 5 wt%, and 9 wt%
Polarization	-0.05 ~ -0.1 V *vs.* OCP

Procedure for FeCO$_3$ Precipitation Rate Calculation

The methodology of calculating the precipitation rate of corrosion product from EQCM measurement is illustrated in Figure 6 by using $FeCO_3$ precipitation at 80°C as an example. During the test, the pH value and [Fe^{2+}] in the bulk solution were measured multiple times to obtain the saturation value of $FeCO_3$ according to Equation (1). Due to the uncertainties associated with measurements of the bulk pH and [Fe^{2+}], an estimation of the error in determining S_{FeCO_3} was made. Given that the accuracy of measuring the pH was found to be approximately 0.1 pH unit and the error in the [Fe^{2+}] measurement was up to 1% of the measurement range, a 12% error in determining S_{FeCO_3} can be expected. The corresponding error bars were added to all the graphs below. The error in measuring the mass change due to precipitation using the EQCM was so small that it cannot be shown adequately on the plots below (the error bars are much smaller than the size of the symbols used).

Figure 6 shows that the mass change monitored by EQCM increased due to the precipitation on the surface of the quartz crystal. Based on this information, the instantaneous slope (mass change per unit area *vs.* time) at those specific times was calculated and used to determine the precipitation rates of $FeCO_3$ (PR_{FeCO_3}) at their corresponding saturation value. The precipitation rates measured by EQCM with the units of μg/(cm²·s) were converted to mol/(m²·s). Even though the precipitation is a two-step process that includes both the nucleation and growth, this current research aims at finding only the rate of crystal growth.
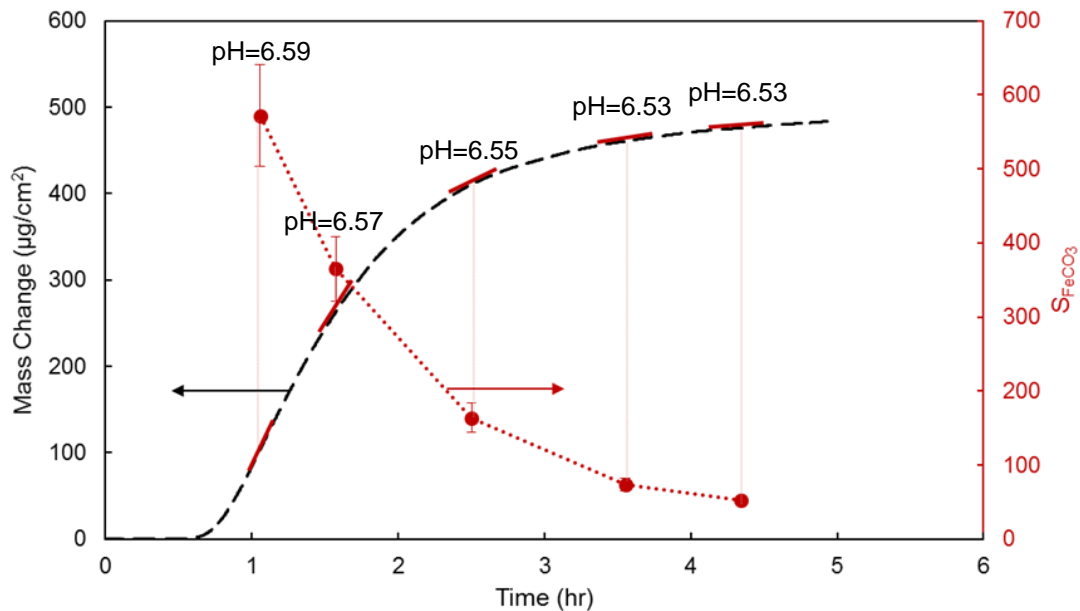
Figure 6: Illustration of FeCO₃ precipitation rate calculation. pH 6.6, Initial S(FeCO₃)=600, 80°C, 1 wt% NaCl, and 0.53 bar CO₂.

EXPERIMENTAL RESULTS AND DISCUSSION

As illustrated in the section of Procedure for FeCO3 Precipitation Rate Calculation, both of the PR_{FeCO_3} and its corresponding S_{FeCO_3} were obtained from laboratory measurements. This leaves $k_{r,FeCO_3}$ and ΔG_{FeCO_3} the only two unknowns in Equation (4) as the temperature is a known value, and the $K_{sp,FeCO_3}$ is calculated according to Equation (2) based on experimental conditions. To extract values for $k_{r,FeCO_3}$ and ΔG_{FeCO_3}, the precipitation rate of FeCO₃ needs to be measured at different temperatures in addition to the ones measured at 80°C.

In this section, PR_{FeCO_3} measured from 1 wt%, 3 wt%, 5 wt%, and 9 wt% NaCl solutions are compared with Z. Ma's FeCO₃ precipitation rate model[9] at 60°C and 70°C. The values for $k_{r,FeCO_3}$ and ΔG_{FeCO_3} are extracted based on these experiment results. The relationship between the ionic strength of the solution, and the $k_{r,FeCO_3}$ and ΔG_{FeCO_3} values are discussed before proposing an improved FeCO₃ precipitation rate model that considers the solution non-ideality effect on both $k_{r,FeCO_3}$ and ΔG_{FeCO_3}.

The model predictions using values of $k_{r,FeCO_3}$ and ΔG_{FeCO_3} calibrated from 1 wt.% NaCl solution are plotted and compared with measured results from different NaCl concentrations at 60°C (Figure 7) and 70°C (Figure 8). Similar to what has been shown in Figure 3, the model seems to predict the correct trend, i.e., both the predicted and measured PR_{FeCO_3} increased in more concentrated NaCl solutions. However, a deviation between the predicted values and measurement values exists and it becomes more obvious in solutions with higher NaCl content. This is not surprising given to the fact that the $k_{r,FeCO_3}$ and ΔG_{FeCO_3} used in Z. Ma's model were extracted from a solution with a relatively low NaCl concentration.
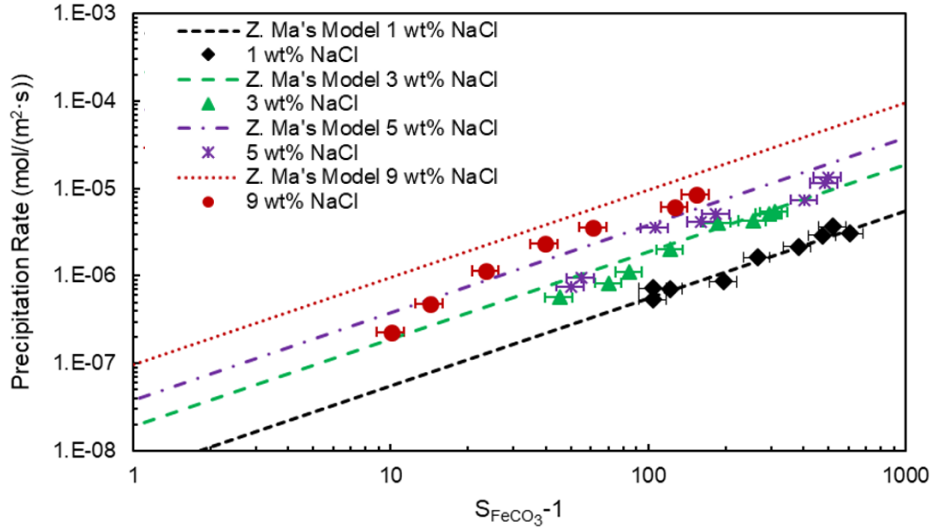
Figure 7. Comparison between model's predictions and measured results in solutions with different NaCl concentrations at 60°C, initial pH=6.60, and 0.81 bar CO_2.
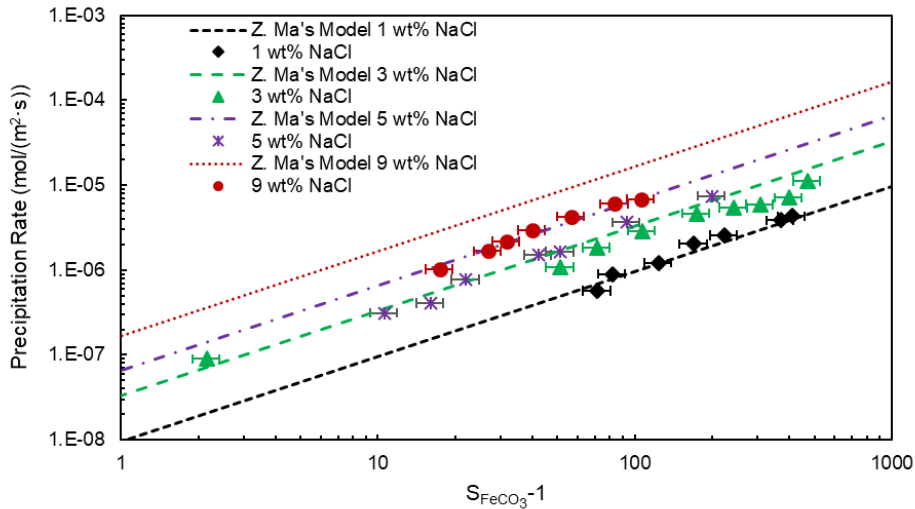

Figure 8. Comparison between model's predictions and measured results in solutions with different NaCl concentrations at 70°C, initial pH=6.60, and 0.69 bar CO_2.

Based on the measurements, the two parameters in Equation (4), $k_{r,FeCO_3}$ and ΔG_{FeCO_3}, can be re-calibrated by applying a natural logarithm on both sides of the precipitation rate equation. To aid in analysis, Equation (6) was derived from Equation (4):

$$ln \frac{PR_{FeCO_3}}{K_{sp,FeCO_3} \cdot (S_{FeCO_3} - 1)} = -\frac{\Delta G_{FeCO_3}}{RT} + ln \, k_{r,FeCO_3} \tag{6}$$

When plotting $ln \frac{PR_{FeCO_3}}{K_{sp,FeCO_3} \cdot (S_{FeCO_3} - 1)}$ vs. $(-\frac{1}{RT})$, the activation energy ΔG_{FeCO_3} can be obtained from the slope of the straight line and $\ln k_{r,FeCO_3}$ can be determined from the y-intercept. By using the average experimental value at each temperature, the best fit line yielded ΔG_{FeCO_3} =73739 $J \cdot mol^{-1}$ and $k_{r,FeCO_3}$=3.32×10^7 $m^4 \cdot mol^{-1} \cdot s^{-1}$ as shown in Figure 9 for 1 wt% NaCl.[9.] The corresponding values of these two kinetic parameters extracted from all four measured conditions are summarized in Table 2 by applying the same methodology. It is important to notice that the ionic strength affects both ΔG_{FeCO_3} and $k_{r,FeCO_3}$ as their values decrease in more concentrated solutions. In addition to that, the $k_{r,FeCO_3}$ decreased much more (about 20 times) than the decrease of ΔG_{FeCO_3} (about 10%) when the NaCl concentration was increased from 1 wt% to 9 wt%.

$$\ln \frac{PR_{FeCO_3}}{K_{sp,FeCO_3}(S_{FeCO_3} - 1)} = 73739 \left(-\frac{1}{RT}\right) + 31.135$$
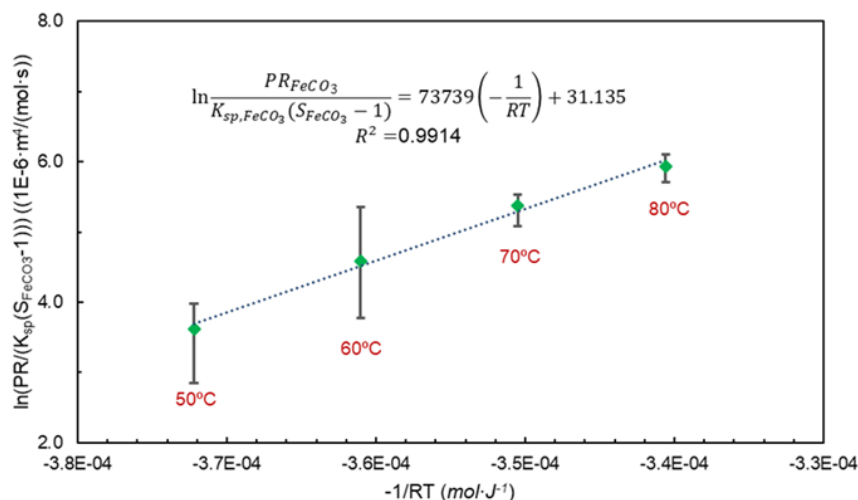$$R^2 = 0.9914$$

Figure 9. Best fit line for activation energy and kinetic constant in the FeCO₃ precipitation rate equation. Adapted from Ma *et al.*[9].

Table 2
Extracted ΔG_{FeCO_3} and $k_{r,FeCO_3}$ in non-ideal solutions.

wt% NaCl	Ionic strength $mol \cdot L^{-1}$	ΔG_{FeCO_3} $kJ \cdot mol^{-1}$	$k_{r,FeCO_3}$ $m^4 \cdot mol^{-1} \cdot s^{-1}$
1	0.17	73.7	3.32 × 10^7
3	0.52	71.3	1.12 × 10^7
5	0.86	70.7	6.35 × 10^6
9	1.73	67.5	1.59 × 10^6

ΔG_{FeCO_3} and $k_{r,FeCO_3}$ are plotted against ionic strength in Figure 10 and Figure 11 to further investigate their behavior in non-ideal solutions. The best fit line suggests that the ΔG_{FeCO_3} is linearly dependent on the ionic strength, and the $k_{r,FeCO_3}$ is exponentially dependent on it. This leads to the development of a new precipitation rate equation for FeCO₃ as shown in Equation (7). It follows the same format as Equation (4), yet the effect of ionic strength on both ΔG_{FeCO_3} and $k_{r,FeCO_3}$ are now considered with $k_{r,FeCO_3} = 4 \times 10^{13} e^{-1.9I}$ and $\Delta G_{FeCO_3} = -3800I + 74000$, as illustrated in Figure 10 and Figure 11.

$$PR_{FeCO_3} = (4 \times 10^{13} e^{-1.9I}) \exp\left(\frac{3800I - 74000}{RT}\right) K_{sp,FeCO_3}(S_{FeCO_3} - 1) \tag{7}$$
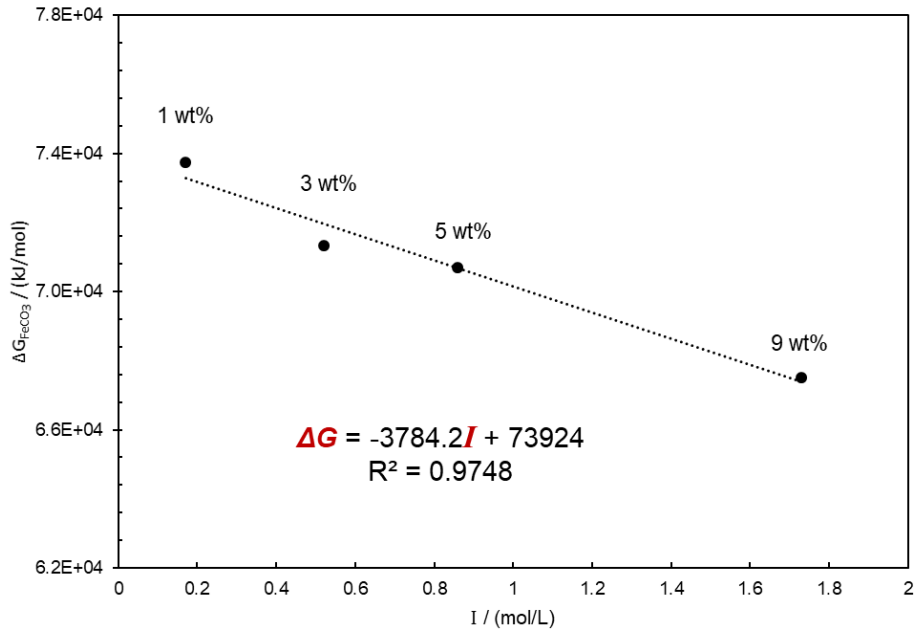

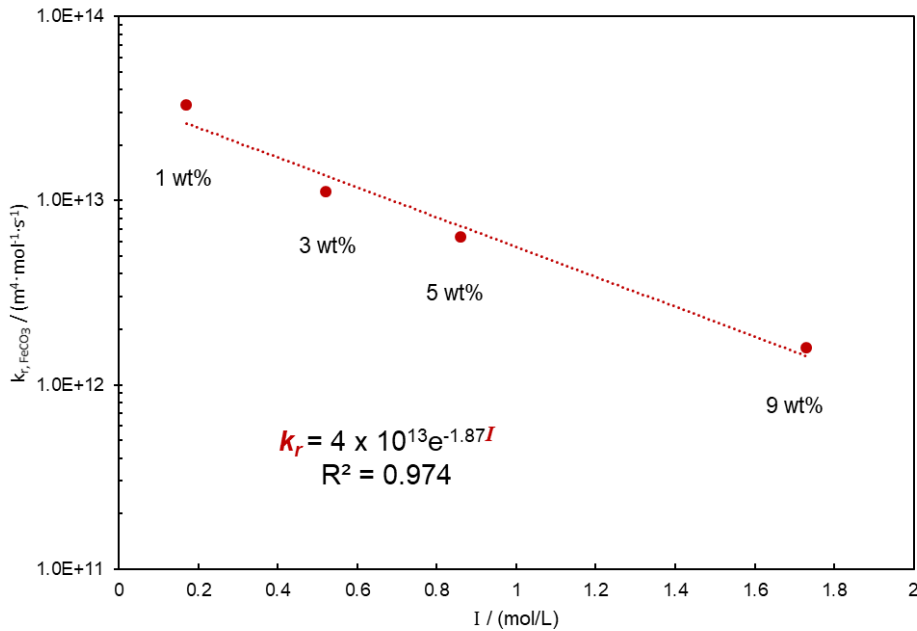**Figure 10: Extracted activation energy *vs.* ionic strength in linear scale.**

Figure 11. Extracted kinetic constant *vs.* ionic strength in semi-logarithm scale.

11

The parity plots that compares the experimental $FeCO_3$ precipitation rate data with the calculated $FeCO_3$ precipitation rate data are shown in Figure 12 for the original model where ΔG_{FeCO_3} and $k_{r,FeCO_3}$ are constants[9] (left) and the current model with the new ionic strength dependent correlations (right). In an ideal case, all the points should fall onto the diagonal. One can see that the points on the right plot distribute much more evenly around the diagonal line, indicating a better fit.
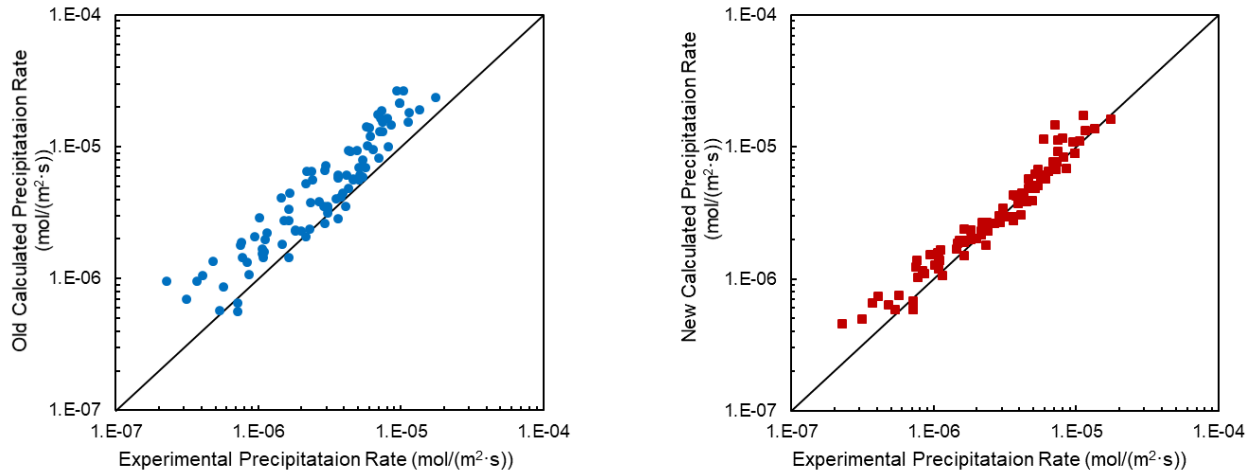

Figure 12. Parity plot comparison of experimental precipitation rate and the calculated precipitation rate using original Z Ma's model (left) and current improved model (right).

CONCLUSIONS

- Previously used $FeCO_3$ precipitation kinetics related parameters were only validated in solution with 1 wt% NaCl, which led to an over estimation of $FeCO_3$ precipitation kinetics in solutions with higher ionic strength.
- In this project, both ΔG_{FeCO_3} and $k_{r,FeCO_3}$ were calculated from experiments in more concentrated NaCl solutions, and it was shown that the non-ideality affects both parameters.
- A kinetic model of $FeCO_3$ precipitation considering the effect of ionic strength was proposed.

ACKOWLEDGEMENTS

REFERENCE

1   S. Nesic and W. Sun, "Corrosion in acid gas solutions," in *Shreir's Corrosion*, Oxford: Elsevier, pp. 1270-1298, 2010.

2   W. Sun, "Kinetics of Iron Carbonate and Iron Sulfide Scale Formation in CO_2/H_2S Corrosion," Ph.D. Dissertation, Dept. Chem. Eng., Ohio Univ., Athen, OH, 2006.

3   B. Brown, K.-L. J. Lee, and S. Nesic, "Corrosion in multiphase flow containing small amounts of H_2S," CORROSION 2003, paper no. 03341, (Houston, TX, 2004).

4   J. Ning, Y. Zheng, B. Brown, D. Young, and S. Nesic, "Construction and Verification of Pourbaix Diagrams for Hydrogen Sulfide Corrosion of Mild Steel," CORROSION/2015, paper no. 5507, (Dallas, Texas, 2015).

5   E. W. J. v. Hunnik, B. F. M. Pots, and E. L. J. A. Hendriksen, "The Formation of Protective $FeCO_3$ Corrosion Product Layers In CO_2 Corrosion," CORROSION 1996, paper no. 6, (Houston, TX, 1996).

6   J. Greenberg and M. Tomson, "Precipitation and dissolution kinetics and equilibria of aqueous ferrous carbonate *vs.* temperature," *Applied Geochemistry* 7,(1992): pp. 185-190.

7   M. L. Johnson and M. B. Tomson, "Ferrous Carbonate Precipitation Kinetics and its Impact on CO_2 Corrosion," CORROSION 1991, paper no. 268, (Houston, TX, 1991).

8   W. Sun and S. Nesic, "Kinetics of corrosion layer formation: part 1—iron carbonate layers in carbon dioxide corrosion," *Corrosion* 64,(2008): pp. 334-346.

9   Z. Ma, Y. Yang, B. Brown, S. Nesic, and M. Singer, "Investigation of precipitation kinetics of $FeCO_3$ by EQCM," *Corrosion Science* 141,(2018): pp. 195-202.

10   G. Sauerbrey, "Verwendung von Schwingquarzen zur Wägung dünner Schichten und zur Mikrowägung," *Zeitschrift für physik* 155,(1959): pp. 206-222.

11   R. Baboian, *Corrosion Tests and Standards: Application and Interpretation*, Second ed. (West Conshohocken, PA: ASTM International, 2005), p. 141.